

## Supplementary Information (SI)

### Force Spectroscopy reveals the effect of different ions in the nanomechanical behavior of phospholipid model membranes: the case of potassium cation

Redondo-Morata, Lorena<sup>1,2,3</sup>, Oncins, Gerard<sup>4</sup>, Sanz, Fausto<sup>1,3,2\*</sup>

<sup>1</sup>Institute for Bioengineering of Catalonia (IBEC), 15-21 Baldiri I Reixac, 08028, Barcelona, Spain

<sup>2</sup>Physical Chemistry Department, University of Barcelona (UB), 1-3 Martí i Franquès, 08028, Barcelona, Spain

<sup>3</sup>CIBER de Bioingeniería, Biomateriales y Nanomedicina (CIBER-BBN), Campus Río Ebro, Edificio I+D, Poeta Mariano Esquillor s/n, 50018 Zaragoza, Spain

<sup>4</sup>Scientific and Technological Centers, University of Barcelona (SCT-CCiTUB), 1 Soler i Sabarís, 08028, Barcelona, Spain

\*Corresponding author: fsanz@ub.edu

#### 1. DLVO calculation for a conical tip-flat substrate geometry

According to the DLVO theory and using the calculated values  $\sigma$  of the AFM tip ( $\sigma_{tip}$ ) and the  $\sigma$  of the SPB ( $\sigma_{sample}$ ), the DLVO interaction between the two surfaces as the tip approaches the bilayer can be calculated by summation of the van der Waals forces with the electrostatic forces. The theoretical DLVO model for a conical tip-flat substrate geometry was described by Drelich *et al.* (1, 2), and as aforementioned, consists on the summation of the van der Waals forces

$$F^{vdW} = \frac{A}{6} \left[ \frac{(R+D)-2L_1}{L_1^2} - \frac{R-D}{D^2} \right] - \frac{A}{3 \tan^2 \alpha} \left( \frac{1.0}{L_1} + \frac{(R \sin \alpha \tan \alpha) - D - R(1 - \cos \alpha)}{L_1^2} \right) \quad (S1)$$

with the electrostatic forces, where equation S2 considers the system has a constant  $\sigma$ :

$$F^{edl} = \frac{4\pi}{\epsilon_0 \epsilon \kappa^2} \sigma_{tip} \sigma_{sample} (a_0 e^{-\kappa D} - a_1 e^{-\kappa L_1}) + \frac{2\pi}{\epsilon_0 \epsilon \kappa^2} (\sigma_{tip}^2 + \sigma_{sample}^2) (a_2 e^{-2\kappa D} - a_3 e^{-2\kappa L_1}) + \frac{4\pi}{\epsilon_0 \epsilon \kappa \tan \alpha} \left[ b_1 \sigma_{tip} \sigma_{sample} e^{-\kappa L_1} + b_2 \frac{(\sigma_{tip}^2 + \sigma_{sample}^2)}{2} e^{-2\kappa L_1} \right] \quad (S2)$$

where  $L_1 = D + R(1 - \cos \alpha)$ ,  $a_0 = \kappa R - 1$ ,  $a_1 = \kappa R \cos(\alpha - 1)$ ,  $a_2 = a_0 + 0.5$ ,  
 $a_3 = a_1 + 0.5$

$$b_1 = \left[ R \sin \alpha - \frac{D + R(1 - \cos \alpha)}{\tan \alpha} \right] + \frac{1}{\tan \alpha} \left[ \left( L_1 + \frac{1}{\kappa} \right) \right]$$

$$b_2 = \left[ R \sin \alpha - \frac{D + R(1 - \cos \alpha)}{\tan \alpha} \right] + \frac{1}{\tan \alpha} \left[ \left( L_1 + \frac{1}{2\kappa} \right) \right]$$

$\alpha$  and  $\beta$  are the geometrical angles for the spherical cap at the tip end and conical tip with  $\alpha + \beta = 90^\circ$ ,  $A$  is the non-retarded Hamaker constant ( $A = 10^{-21}$  J (3)),  $D$  is the distance from the end of the tip to the substrate,  $L$  is the distance between a differential surface section of the tip to the substrate,  $R$  is the radius of the spherical cap at the tip end,  $\epsilon$  is the dielectric constant of the solution of the system,  $\epsilon_0$  is the vacuum permittivity,  $1/\kappa$  is the Debye length ( $7.84 \cdot 10^{-10}$  m),  $\sigma_{tip}$  and  $\sigma_{sample}$  are the surface charge density for the tip and the sample, respectively.

In our experiments pyramid-shape tips were used. For this calculation, the tip can be approximated as conical with a spherical cap at its apex. The equations used (S1 and S2) require the calculation of  $\alpha$  and  $\beta$ , angles which were experimentally assessed by means of scanning electron microscopy image of the AFM tip ( $\alpha = 38^\circ$  and  $\beta = 52^\circ$ ). The deconvolution of the AFM tip radius with SPIP 4.4.3.0 software (Image Metrology, Lyngby, Denmark) was performed using a calibration array (Aurora NanoDevices Inc., Nanaimo, BC, Canada), obtaining a  $R$  value of 9 nm. All the AFM tips used in this work were previously deconvoluted with the aforementioned procedure and only those with a  $R$  value ranging from 8-10 nm were used improved geometrical consistency. Figure S1 shows a scheme where all the parameters used in Drelich *et al.* modeling (1) are shown.

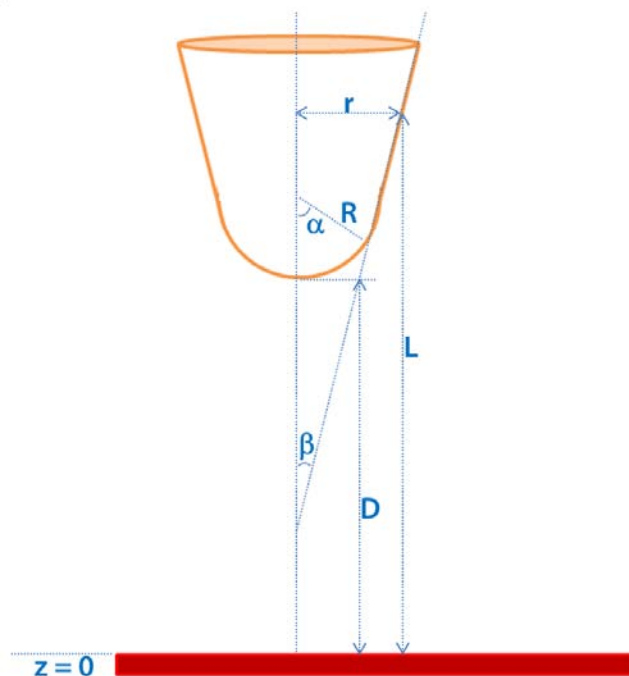


**Figure S1.** Geometry of the interaction between a conical tip and a flat surface system as described by Drelich *et al.* (1).  $\alpha$  and  $\beta$  are the geometric angles for the spherical cap at the tip end and the conical tip with  $\alpha + \beta = 90^\circ$ ;  $D$  is the distance between the tip end and the substrate,  $L$  is the distance between a differential surface section of the tip and the substrate,  $r$  is the radius of the circle of the tip at a given vertical position,  $R$  is the radius of the spherical cap at the tip end.

## 2. Surface charge density of lipid membranes

**Table S1.**  $\xi$ -potential values of the DPPC and DLPC liposomes depending on the cation present in the measuring solution. Every value is the average of 3 measurements performed with 3 independent samples. Error stands for standard deviation value within the measurements. Buffer solutions correspond to 150 mM of the electrolyte and blank experiment corresponds to measurements in pure water.

| $\xi$ -potential (mV) | $\text{Li}^+$    | $\text{Na}^+$    | $\text{K}^+$      | $\text{Cs}^+$    | TEA             | Blank            |
|-----------------------|------------------|------------------|-------------------|------------------|-----------------|------------------|
| DPPC                  | $-0.33 \pm 0.23$ | $-5.47 \pm 1.7$  | $-5.19 \pm 0.68$  | $-7.53 \pm 1.12$ | $-5.68 \pm 0.4$ | $-16.7 \pm 3.87$ |
| DLPC                  | $-5.52 \pm 0.26$ | $-9.19 \pm 0.38$ | $-11.15 \pm 0.35$ | $-9.11 \pm 5.22$ | $-14.5 \pm 0.9$ | $-43.5 \pm 2.56$ |

In order to calculate the  $\sigma$  values of the liposomes from the experimentally measured  $\xi$ -potential values, the simplified Grahame equation for low potentials can be applied (equations S3 and S4):

$$\sigma = \varepsilon\varepsilon_0 k\psi_0 \quad (\text{S3})$$

$$\psi_0 \cong \xi \quad (\text{S4})$$

where  $k$  stands for the reciprocal of the Debye length ( $\lambda$ ) and  $\psi_0$  is the surface potential. The  $\xi$ -potential is often approximated to the  $\psi_0$ , as the former stands for the charge at the point where the diffuse layer ends, that is, the slipping plane.

### 3. Continuum nucleation model

Under constant velocity conditions, the continuum nucleation model leads to an expression for the probability,  $P(F_y)$ , of measuring a certain breakthrough  $F_y$  value, which is described by:

$$\ln P(F_y) = -\frac{A}{K \cdot v} \int_{F_s}^{F_y} \exp\left(-\frac{c}{F_y' - F_s}\right) dF_y' \quad (\text{S5})$$

$$c = \frac{2\pi^2 R\Gamma^2}{k_B T}$$

$$F_s = 2\pi RS$$

where  $A$  can be approximated to the resonance frequency of the cantilever,  $k_B$  is the Boltzmann constant,  $T$  is the temperature,  $R$  is the AFM probe tip radius and  $K$  is the spring constant of the AFM probe.

Equation S5 can be analytically integrated and  $dP/dF$  can be calculated using:

$$\frac{dP}{dF_y} = \frac{A}{K \cdot v} \exp\left\{-\frac{c}{F_y - F_s} - \frac{A}{K \cdot v} \left[ \exp\left(-\frac{c}{F_y - F_s}\right) (F_y - F_s) - c \text{Ei}\left(\frac{c}{F_y - F_s}\right) \right]\right\} \quad (\text{S6})$$

$$\text{Ei} = \int_x^\infty \frac{e^{-t}}{t} dt$$

Fitting the equation S6, with 3 unknown parameters ( $A$ ,  $\Gamma$  and  $S$ ), to the experimental force distributions obtained for the probed PC phospholipids (DLPC and DPPC) while varying the electrolytes present in aqueous solution provides values for  $\Gamma$  and  $S$ . Figure S2A) and S2B) show the variation of  $\Gamma$  and  $S$  as a function of the cation present in the buffer solution, respectively. While the values for  $\Gamma$  do not significantly vary with the cation solution,  $S$  values change

slightly, suggesting that certain buffer solutions modify the mesoscopic behavior of the film, especially in the case of DPPC.

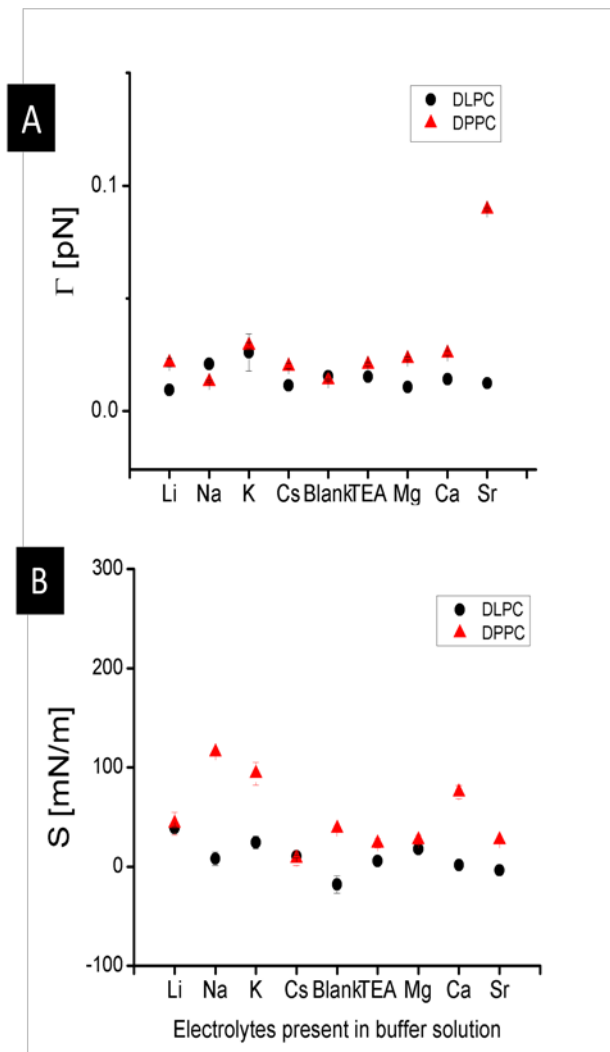


**Figure S2. Fitting parameters from the continuum nucleation model.** (A) Variation of the line tension, and (B) Variation of the spreading pressure,  $S$ , as a function of electrolyte present in the aqueous environment, where error bars stand for standard error.

#### 4. Force Spectroscopy on lipid model membranes: DPPC and DLPC

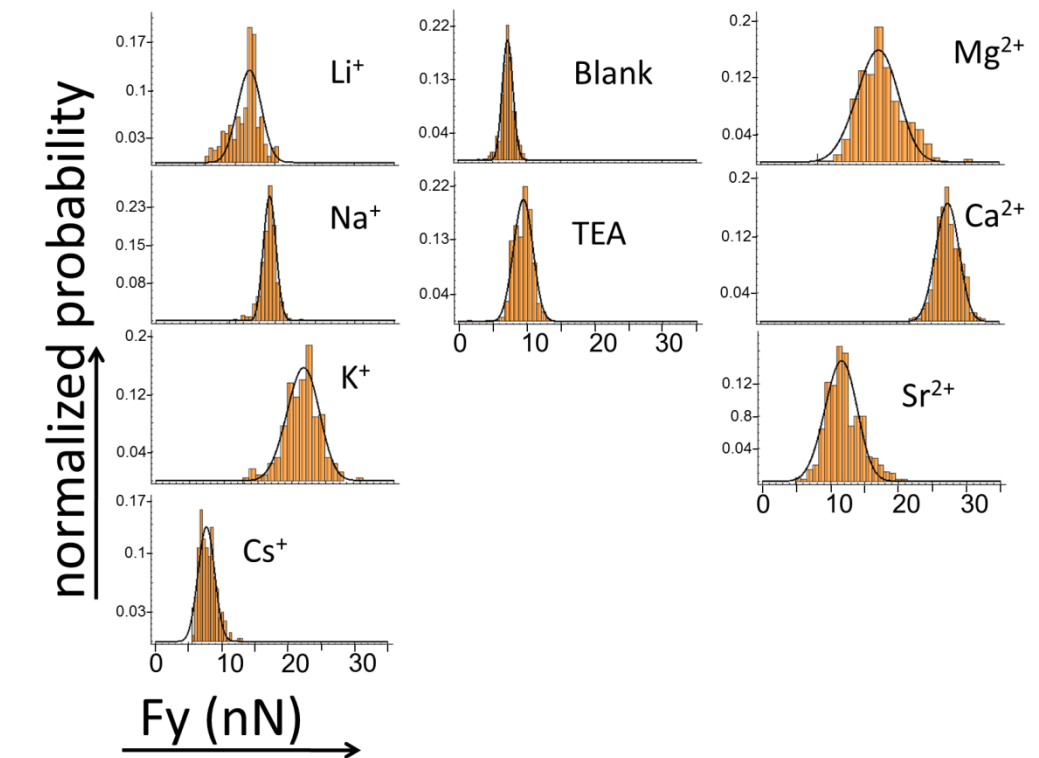


**Figure S3. Histograms** corresponding to the  $F_y$  values for DPPC bilayers under different ionic compositions: Li<sup>+</sup>, Na<sup>+</sup>, K<sup>+</sup>, Cs<sup>+</sup>, blank (consisting on pure water), TEA, Mg<sup>2+</sup>, Ca<sup>2+</sup> and Sr<sup>2+</sup>. Black solid line represents the fitting to the continuum nucleation model.

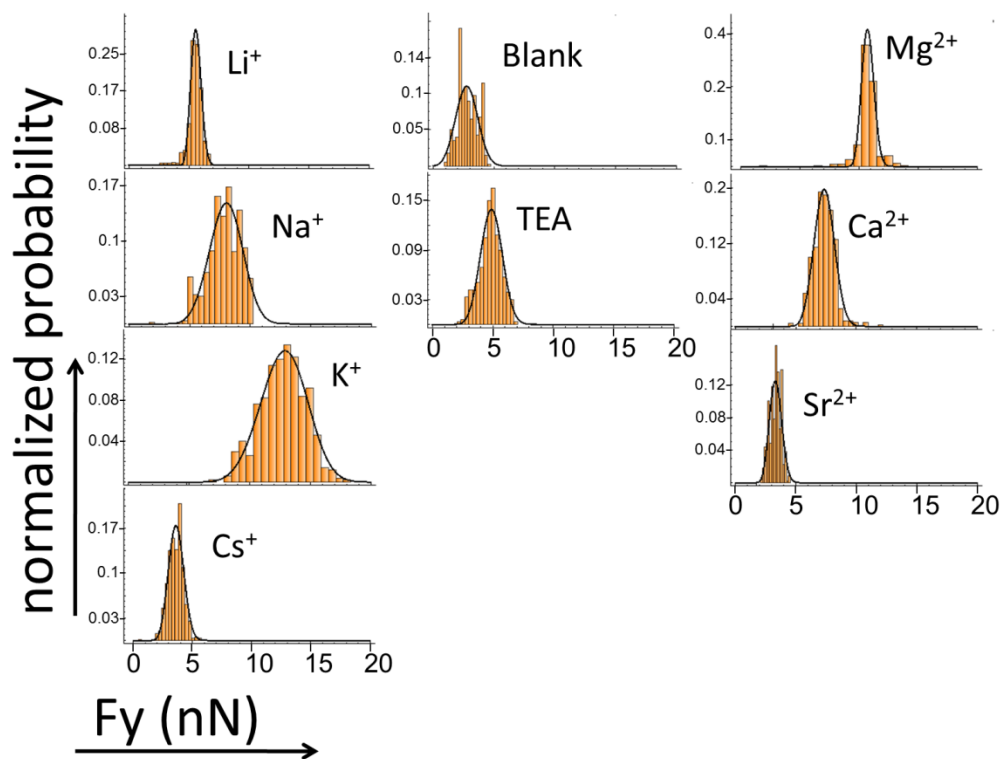


**Figure S4. Histograms** corresponding to the  $F_y$  values for DLPC bilayers under different ionic compositions:  $\text{Li}^+$ ,  $\text{Na}^+$ ,  $\text{K}^+$ ,  $\text{Cs}^+$ , blank (consisting on pure water), TEA,  $\text{Mg}^{2+}$ ,  $\text{Ca}^{2+}$  and  $\text{Sr}^{2+}$ . Black solid line represents the fitting to the continuum nucleation model.

### 5. Dependence of the $F_y$ on loading rate

It is well established that  $F_y$  value depend on the loading rate (4-7). As different cations give rise to different  $F_y$  value at a fixed tip velocity, it is conceivable to think that the presence of different ions will result on a different kinetic rate for the rupture process. In a recent work, Sullan *et al.* used the loading rate dependence of the  $F_y$  value to calculate differences in the activation energy for the rupture process as a function of the cholesterol content (7). In order to test the rate dependence of the  $F_y$  value, Figure S5 shows the experimental  $F_y$  value measured as a function of three different loading rates ( $0.1$ ,  $1$  and  $10 \mu\text{m}\cdot\text{s}^{-1}$ ). We provide data both for DPPC and DLPC in the presence of  $\text{Na}^+$  and  $\text{K}^+$ . In both cases, the  $F_y$  rate dependence is flatter for  $\text{Na}^+$  than for  $\text{K}^+$ . These results confirm the fact that both  $\text{Na}^+$  and  $\text{K}^+$  modify the kinetics of the rupture process, leading to different activation energy. This is in accordance to the continuum nucleation model, where the lipid bilayer rupture is described as a two-state process with a single energy barrier.

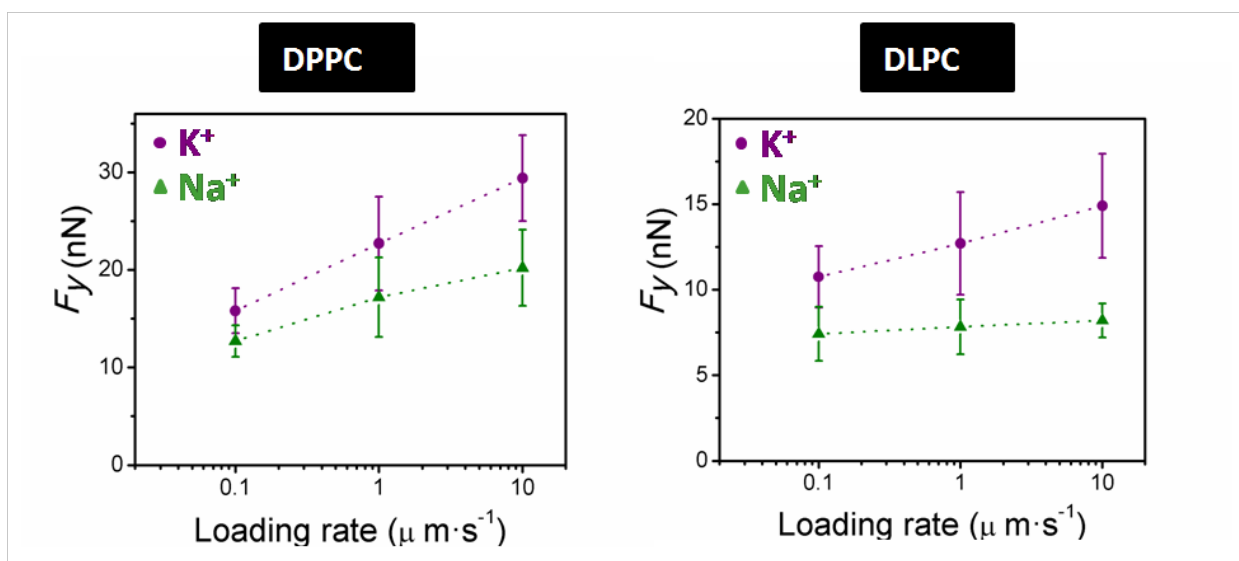


**Figure S5.** Dependence of the  $F_y$  on loading rate for Left) DPPC and Right) DLPC in the presence of two different cations,  $\text{K}^+$  (violet circles) and  $\text{Na}^+$  (green triangles).

## References

1. Drelich, J., J. Long, and A. Yeung. 2007. Determining surface potential of the bitumen-water interface at nanoscale resolution using atomic force microscopy. *Canadian Journal of Chemical Engineering* 85:625-634.
2. Yin, X. H., and J. Drelich. 2008. Surface charge microscopy: Novel technique for mapping charge-mosaic surfaces in electrolyte solutions. *Langmuir* 24:8013-8020.
3. Israelachvili, J. N. 1992. *Intermolecular and Surface Forces*. Academic Press, London.
4. Butt, H. J., and V. Franz. 2002. Rupture of molecular thin films observed in atomic force microscopy. I. Theory. *Physical Review E* 66.
5. Loi, S., G. Sun, V. Franz, and H.-J. Butt. 2002. Rupture of molecular thin films observed in atomic force microscopy. II. Experiment. *Phys Rev E Stat Nonlin Soft Matter Phys* 66:031602.
6. Franz, V., S. Loi, H. Muller, E. Bamberg, and H. H. Butt. 2002. Tip penetration through lipid bilayers in atomic force microscopy. *Colloids and Surfaces B-Biointerfaces* 23:191-200.
7. Sullan, R. M. A., J. K. Li, C. C. Hao, G. C. Walker, and S. Zou. 2010. Cholesterol-Dependent Nanomechanical Stability of Phase-Segregated Multicomponent Lipid Bilayers. *Biophysical Journal* 99:507-516.